Hindawi
Shock and Vibration
Volume 2021, Article ID 9972981, 12 pages
https://doi.org/10.1155/2021/9972981

Research Article

Characteristics of Typhoon "Fung-Wong" Near Earth Pulsation

Xiujun Li,[1] **Yongguang Li**,[1] **Jianting Zhou**,[1] **Qian Wang**,[2] **and Xu Wang**[1]

[1]*State Key Laboratory of Mountain Bridge and Tunnel Engineering, Chongqing Jiaotong University, Chongqing 400074, China*
[2]*Department of Chemical and Environmental Engineering, Chongqing University of Arts and Science, Chongqing 402160, China*

Correspondence should be addressed to Jianting Zhou; jtzhou@cqjtu.edu.cn

Received 12 March 2021; Accepted 12 June 2021; Published 19 June 2021

Academic Editor: Fuyou Xu

To study the wind field characteristics near the ground pulsation in typhoon conditions, wind field conditions in the area affected by Typhoon "Fung-Wong" were monitored using wind field instruments installed in the construction building of Wenzhou University, China. Real-time wind field data were collected during typhoons. Wind characteristic parameters such as mean wind speed, wind direction angle, turbulence intensity, gust factor, peak factor, coherence function, and autocorrelation were analyzed, and the wind field characteristics during the typhoon were summarized. The results indicated that the longitudinal and lateral turbulence intensities decreased with an increase in the mean wind speed, and there was an obvious linear relationship between them. The vertical and horizontal gust factor and peak factor decreased with an increase in mean wind speed, and the trend was more obvious in the horizontal direction. There was a significant correlation between the gust factor and the peak factor. The turbulence intensity and gust factor decreased with time, and the turbulence intensity attenuation speed increased with time. The empirical curve presented by Davenport (1961) can simulate the correlation characteristics of the fluctuating wind speed components of Typhoon Fung-Wong at some measuring points. With an increase in the time difference, the dependence of the instantaneous values at the two time points gradually decreased.

1. Introduction

Wind disasters exhibit high frequency, large secondary effects, and a wide range of influence, with considerable adverse effects on daily life and the social economy. Wind disasters are the main cause of human casualties and damage to low-rise buildings [1–3]. However, wind resistance research on low-rise buildings has not been sufficient; thus, it is of great practical importance to study the action mechanism and wind field characteristics of low-rise buildings in strong wind conditions [4–6].

Wind always exhibits randomness [7–9]. The randomness is presented as complex turbulence at a given time, with random variations in wind characteristics [10]. To better simulate the randomness of wind, ASCE in America, NBCC in Canada, BSI in England, SAA in Australia, EuroCode and ESDU in Europe, and JS in Japan have studied and formulated design codes based on climate, economy, terrain, and other related factors [5, 11]. Computational fluid dynamics (CFD) is a numerical method used to analyze wind characteristics [12, 13]. Cochran and Derickson believed that it is critical for numerical inflow boundary conditions to match the mean and turbulent inflow conditions in the CFD method [14]. Hu et al. proposed a new form of turbulence kinetic energy profile and studied wind characteristics including mean wind speeds (U), turbulence intensities (I), and mean square deviations [15]. Four subgrid scale (SGS) models and two ground conditions were used for six large-eddy simulation (LES) calculations to analyze the wind characteristics over a hill. The dynamic SGS model results were inconsistent with the experimental results [16, 17]. Focusing on the surface conditions of a hill, Tamura et al. used the LES method to study the turbulent boundary layer flows over a hill and demonstrated the effect of vegetation on turbulence statistics [13]. Most of these studies produced good results. It is difficult to obtain accurate wind data because a typhoon exhibits great uncertainty. Because the actual bridge location was affected by the surrounding terrain, the simulation results were complex and the wind characteristics varied at different locations; thus, a wind

simulation at a specific location had limited value [18, 19]. In addition, as the numerical simulation results were usually validated by wind tunnel tests or field measurements, it was difficult to obtain boundary condition consistency between the numerical model and the wind tunnel/field measurements [12, 20]. When estimating the wind force on a structure, accurate simulation requires a wind characteristic parameter model. Although a numerical wind simulation can simulate a field wind environment to some extent, the simulation results can only be used as an engineering reference after field measurement and correction. Thus, field measurements are essential for understanding the wind characteristics of an area.

In recent years, much wind characteristic measurement research has been conducted, and much experience and data have been accumulated. Eaton and Mayne installed an anemometer on a two-story residential building in the suburb of Aylesbury. The probability distributions, autocorrelations, power spectra, and cross correlations were calculated and analyzed [21]. An analysis of the wind of Hurricane Hugo over North and South Carolina in 1989 was conducted; the general performance of buildings and the applicability of wind design codes were discussed [22]. Kato et al. observed typhoons 8922 and 9011 from 100 m above the ground and obtained wind turbulence measurements using ultrasonic anemometers [23]. Andersen and Løvseth described wind turbulence data on the western coast of Norway and established the Frøya wind characteristic database [24]. Sharma and Richards analyzed the turbulence characteristic parameters of tropical cyclones at different heights and positions above 10 m and compared them with the recommended values of *AS 1170.2-1989* [25]. Hui et al. and others conducted long-term observations from a 50 m high meteorological tower near the Stonecutters Bridge in Hong Kong. The wind profile, turbulence intensity, turbulence integral scale, coherence function, power spectral density of fluctuating wind speed, and other parameters of monsoon and typhoon data were studied. The results showed that the preset wind profile and turbulence intensity profile were applicable [26, 27]. Based on a health monitoring system installed in a super high-rise building in Hong Kong during several typhoons, wind characteristic parameters including turbulence intensity, peak factor, turbulence integral scale, and power spectral density were analyzed and discussed. [28]. Wang et al. studied strong wind data measured by the Runyang suspension bridge health monitoring system. The wind characteristics of Typhoon Matsa, Typhoon Khanun, and northern winds were analyzed. The variation rules of mean wind speed, wind direction angle, turbulence intensity, turbulence integral scale, and power spectrum were summarized. The results showed that the recommended values of turbulence intensity and turbulence integral scale were not suitable for strong winds, and the Harris model was in good agreement with the measured power spectrum. However, more modified models must be established to meet the measured power spectrum [29]. Zhang et al. studied the influence effect of the wind direction on the wind characteristic of a deep-cut gorge, and the results showed that the wind characteristic parameters changed greatly between different directions [30]. The probabilistic dependence between wind parameters and structural responses was explored by explicit polynomial regression equations using the data of Xihoumen bridge by Liu et al. [31]. Field measurements have other advantages, such as improving wind tunnel test technology and advancing the numerical simulation of typhoons [32–36].

Although wind characteristics research is available for different sites, there is still a lack of research on wind load and wind field characteristics near the surface boundary layer in typhoon wind field conditions. In this study, the real-time wind speed and direction data from Typhoon Fung-Wong were recorded for 13 hours at the top of a building at Wenzhou University in China. Wind characteristic parameters including mean wind speed, wind direction angle, turbulence intensity, gust factor, peak factor, coherence function, and autocorrelation were studied and can be used for data reference in disaster prevention and for structural design of low-rise buildings in typical working conditions in this region.

2. Typhoon Fung-Wong and Its Actual Measurement

The eighth largest tropical storm in 2008 formed on the ocean east of Taiwan at 14 : 00 on August 25 and moved westward under the influence of a Western Pacific subtropical high. It intensified into Typhoon Fung-Wong at 17 : 00 on August 26 and landed at Donghan Town, Fuqing City, Fujian Province, at 22 : 00 on August 28. When it landed, the maximum wind force near the center reached 12, and the wind speed was 33 m/s. It was the strongest typhoon landing in China in 2008, with a high intensity, long influence time, and wide range. The typhoon track is shown in Figure 1.

Two WJ3 anemometers were installed at the top of the fifth building in the construction engineering complex at Wenzhou University in China; complete typhoon data were successfully recorded. The two anemometers were fixed on a straight 9 m high pole, at a total height of approximately 30 m from the ground with a horizontal distance of approximately 17 m between them, as shown in Figure 2. The anemometer sampling frequency was 20 Hz; the wind direction angle was defined as 0° for north and 180° for south. The specific parameters of the anemometers are shown in Table 1.

3. Measured Characteristics of Typhoon Wind Field

3.1. Mean Wind Speed and Mean Wind Direction Angle. The mean wind characteristics include mean wind speed, mean wind direction, and variation of mean wind speed with height. Using the vector decomposition method to process the measured data, the 10-minute mean wind speed and mean wind direction angle during Typhoon Fung-Wong were calculated. We have the following equations:

Figure 1: Route of Typhoon Fung-Wong.

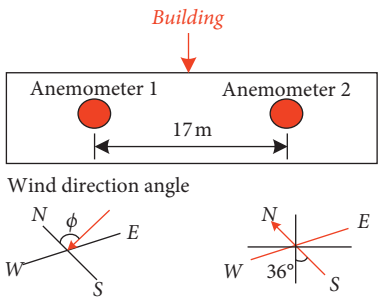

Figure 2: Anemometer layout.

$$U = \sqrt{\overline{v_x(t)}^2 + \overline{v_y(t)}^2}, \tag{1}$$

$$\cos\theta = \overline{v_x(t)}/U, \tag{2}$$

where $\overline{v_x(t)}$ and $\overline{v_y(t)}$ represents the 10-minute average measured two-dimensional wind speed range in the horizontal direction.

The longitudinal fluctuating wind speed and lateral fluctuating wind speed can be obtained according to the mean wind speed (U) and mean wind direction angle (θ), and $u(t)$ and $v(t)$ can be expressed as

$$\begin{aligned} u(t) &= v_x(t)\cos\theta + v_y(t)\sin\theta - U, \\ v(t) &= -v_x(t)\sin\theta + v_y(t)\cos\theta. \end{aligned} \tag{3}$$

The mean wind speed and mean wind direction angle at the east and west measuring points are shown in Figure 3. The measured wind speed and wind direction on both sides were similar, verifying the effectiveness of the measurement. The 10-minute mean wind speed fluctuated from 2 to 10 m/s. The maximum 10-minute mean wind speed at the east measuring point was 10.35 m/s; the maximum 10-minute mean wind speed at the west measuring point was 7.72 m/s. The variation in the mean wind direction angle is concentrated from 10° to 80°; the wind direction angle is relatively stable during the movement of the typhoon. The wind direction angle at the west measuring point is approximately 15° larger than that at the east measuring point, and the fluctuation is more severe.

3.2. Turbulence Intensity. The turbulence intensity is an important index expressing the intensity of wind fluctuation. The turbulence intensity is defined as the ratio of the root mean square of the fluctuating wind speed to the mean wind speed in a basic time interval, expressed as

$$I_i = \sigma_i/U\,(i = u, v), \tag{4}$$

where I_u and I_v are the longitudinal and lateral turbulence intensities, respectively, and σu and σv represent the root mean squares of the longitudinal and lateral fluctuating wind speeds, respectively.

Figure 4 shows the effect of the mean wind speed on the turbulence intensity. It is observed in the figure that the longitudinal and lateral turbulence intensities decrease with an increase in the mean wind speed at the east and west measuring points, and the dispersion at the west measuring point is greater than that at the east measuring point. The average and maximum values of the turbulence intensity and the ratio of the average longitudinal and average lateral turbulence intensities for both sides are presented in Table 2. There is a correlation between the longitudinal and lateral turbulence intensities at the two measuring points. In addition, Table 3 shows the research results of different scholars on turbulence intensity at different bridge sites under strong wind. The results show that the ratio of longitudinal and transverse turbulence intensity is different under different typhoons at various bridge sites, which indicates that different typhoons have uniqueness, and the wind characteristics may be affected by the topography and test environment.

Figure 5 shows the curve of the lateral turbulence intensity versus the longitudinal turbulence intensity with linear fitting. The lateral turbulence intensity increases with an increase in the longitudinal turbulence intensity; there is an obvious positive correlation. The fitting curves of the longitudinal and lateral turbulence intensities at the two measuring points are nearly parallel, which also indicates the effectiveness of the measured turbulence intensity.

In this study, considering the influence of the arrival time on the turbulence intensity, the longitudinal turbulence intensity of the east measuring point is selected as the research object. The change in turbulence intensity at any time

Table 1: Specific parameters of the WJ3 anemometers.

Project	Value
Measurement range of wind speed	0–60 m/s
Measurement accuracy of wind speed	±0.4 m/s
Start-up wind speed	≤0.8 m/s
Resolution of wind speed	0.1 m/s
Measurement range of wind direction	0–359.9°
Measurement accuracy of wind direction	±2°
Resolution of wind direction	1°
Input voltage	AC220 V ± 10% (50 Hz)
Transmission mode	RS485
Transmission distance	1 km
Displayed contents	Instantaneous wind speed/direction, 2-minute mean wind speed/direction, 10-minute mean wind speed/direction

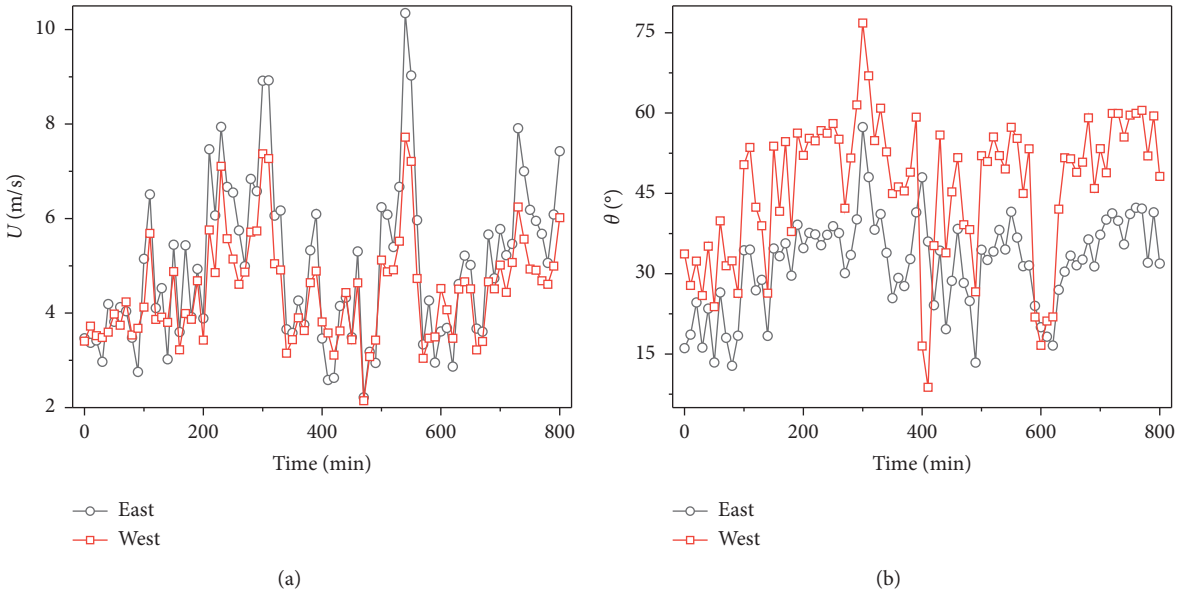

Figure 3: (a) Mean wind speed with time. (b) Wind direction angle with time.

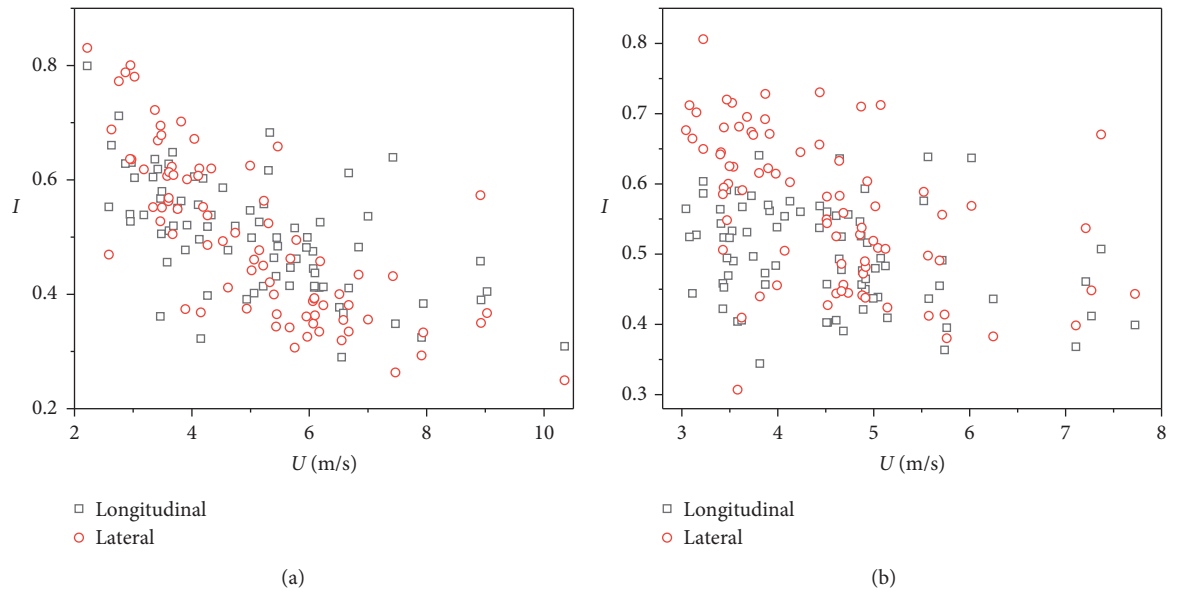

Figure 4: Variation of turbulence intensity with mean wind speed. (a) East measuring point. (b) West measuring point.

Table 2: Average, maximum, and ratio of longitudinal and lateral turbulence intensity at measuring points.

Measuring point	I_u	I_v	max I_u	max I_v	I_u: I_v
East	0.51	0.50	0.80	0.83	1 : 0.98
West	0.50	0.57	0.74	0.93	1 : 1.14

Table 3: Ratio of average longitudinal and transverse turbulence intensity under different typhoons.

Researcher	Bridge site	Typhoon	I_u: I_v
Wang [29]	Runyang bridge	Matsa	1 : 0.81
		Khanun	1 : 1.12
Liu [37–40]	Xihoumen bridge	Rosa	1 : 0.67
Wang [41]	Sutong bridge	Kalmaegi	1 : 0.87
Song [5]	Macao Friendship bridge	Nuri	1 : 0.96

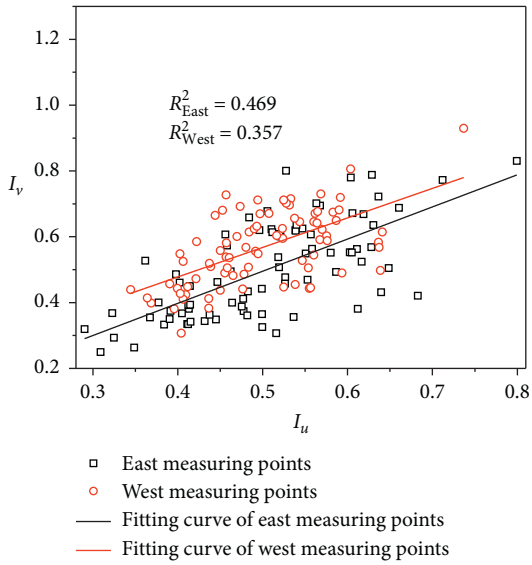

Figure 5: Variation of lateral turbulence intensity with longitudinal turbulence intensity.

with different wind speed conditions is shown in Figure 6, where t_g represents the gust interval. It is observed that, for different wind speed conditions, the turbulence intensity decreases with an increase in distance, and the attenuation coefficient increases with a decrease in turbulence intensity. For the same time interval, the turbulence intensity is greater with a smaller wind speed. Figure 7 shows the change in the mean turbulence intensity at different time intervals in each 1-hour period. The turbulence intensity decreases and its attenuation speed increases with a longer time interval. The polynomial function can be used to fit the variation in the mean turbulence intensity at any time. The mean wind speed was the 1-hour interval wind speed.

3.3. Wind Gust Factor. The gust factor is similar to the turbulence intensity, and it is also an important parameter for characterizing the fluctuation intensity. The gust factor is defined as the ratio of the maximum mean wind speed in all

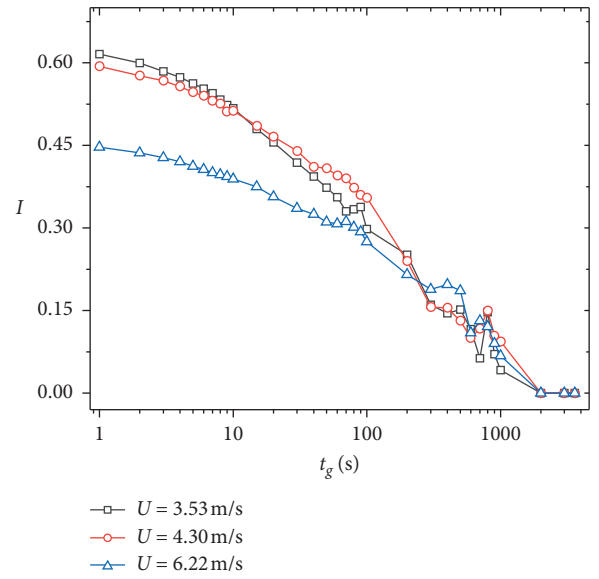

Figure 6: Variation of turbulence intensity at different wind speeds.

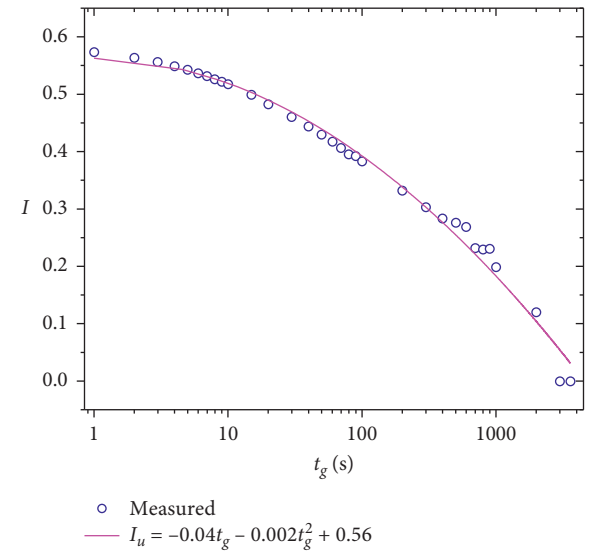

Figure 7: Variation of mean turbulence intensity with time.

directions during the gust duration to the 10-minute mean wind speed, expressed as

$$G_u(t_g) = 1 + \left(\frac{\max\left(\overline{u(t_g)}\right)}{U} \right), \tag{5}$$

$$G_v(t_g) = \max\left(\overline{u(t_g)}\right)/U, \tag{6}$$

where G_u and G_v are the vertical and horizontal gust factors, respectively; $\max(\overline{u(t_g)})$ and $\max(\overline{v(t_g)})$ represent the maximum wind speeds of the longitudinal and lateral fluctuating wind for the gust duration, respectively. Here, t_g is 3 s. The gust factor of Typhoon Fung-Wong passing

through the area was calculated according to equations (5) and (6). The variation in the gust factor with mean wind speed is shown in Figure 8.

Figure 9 shows the relationship between the gust factor and the time interval. The longitudinal and lateral gust factors decrease with time, and the attenuation speed decreases with a decrease in the gust factor. This is different from the conclusion that the turbulence intensity varies with time. The exponential function fitting was conducted according to the change trend of the vertical and horizontal gust factors; the exponential function fitting was $G = at_g^b$. The values of a and b are shown in Table 4.

3.4. Peak Factor. The peak factor represents the instantaneous intensity of fluctuating wind. It is defined as the ratio of the difference between the maximum wind speed and the 10-minute mean wind speed in the gust interval (t_g) and the standard deviation of the pulsating anemometer:

$$gi = \left(U_{t_g} - U\right)/\sigma_i, \quad (i = u, v), \tag{7}$$

where g_u and g_v are the longitudinal and lateral peak factors, respectively, and U_{t_g} and σ_i represent the average maximum wind speed in t_g and the standard deviation of longitudinal fluctuating wind speed, respectively.

Figure 10 shows the variation of peak factor with mean wind speed at the east and west measuring points. It can be seen that the variation trend of peak factor with mean wind speed is very similar to that of gust factor. The average values of longitudinal and lateral peak factors in the east are 2.86 and 0.13, while the average values of longitudinal and lateral peak factors in the west are 2.84 and 0.43. To study the relationship between peak factor and gust factor, the variation curve of gust factor with peak factor is shown in Figure 11. It can be seen from the figure that the longitudinal and lateral gust factors increase with the increase of the peak factor at the points on both sides, and there is an obvious positive correlation between the two parameters. According to the variation trend of gust factor with peak factor, the longitudinal direction and lateral direction are fitted by linear fitting and polynomial function fitting, and then the fitting parameters obtained from the east and west side points are averaged, and the following expression is obtained:

$$\begin{aligned} \text{Longitudinal: } G_u &= 1.01g_u - 0.63, \\ \text{Lateral: } G_v &= -0.76g_v^2 + 3.72g_v - 3.01. \end{aligned} \tag{8}$$

3.5. Coherence Function. The coherence coefficient of fluctuating wind reflects its spatial correlation. Davenport considered that the coherence coefficient followed an exponential function and proposed an empirical expression for the correlation coefficient of fluctuating wind speed [42]:

$$Coh(f) = \exp\left[-\left(\frac{f}{U}\right)\left(C_z^2\Delta z^2 + C_y^2\Delta y^2\right)^{1/2}\right], \tag{9}$$

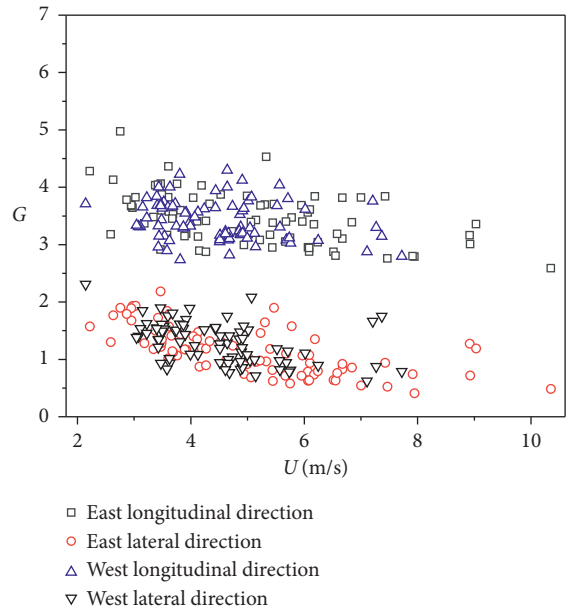

Figure 8: Variation of the gust factor with mean wind speed.

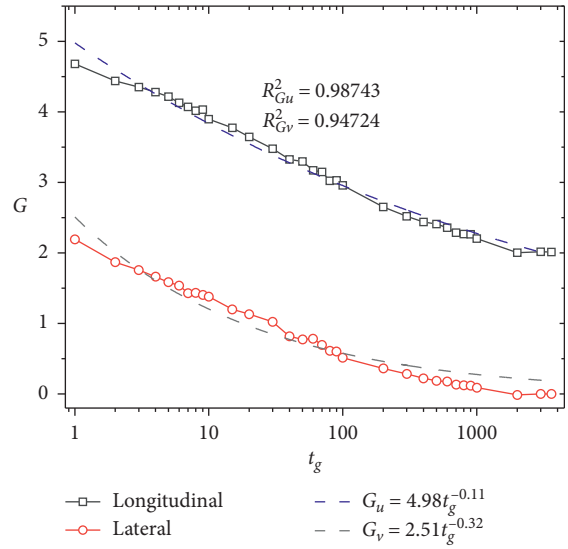

Figure 9: Fitting curve of the mean gust factor with time.

Table 4: Values of constants a and b.

Parameters	Longitudinal	Lateral
a	4.89	2.51
b	−0.11	-0.32

where Δz is approximately 0. Thus, (8) can be simplified as

$$Coh(f) = \exp\left(-\left(\frac{f}{c}\right)C_y\Delta y\right), \tag{10}$$

where Coh (f) and C_y are the coherence and attenuation coefficients, respectively; f and Δy are the frequency and distance between the two anemometers, respectively.

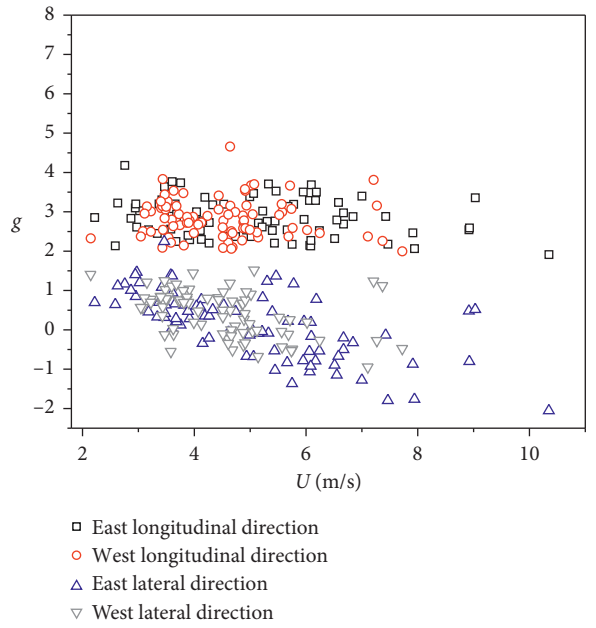

Figure 10: Variation of the peak factor with mean wind speed.

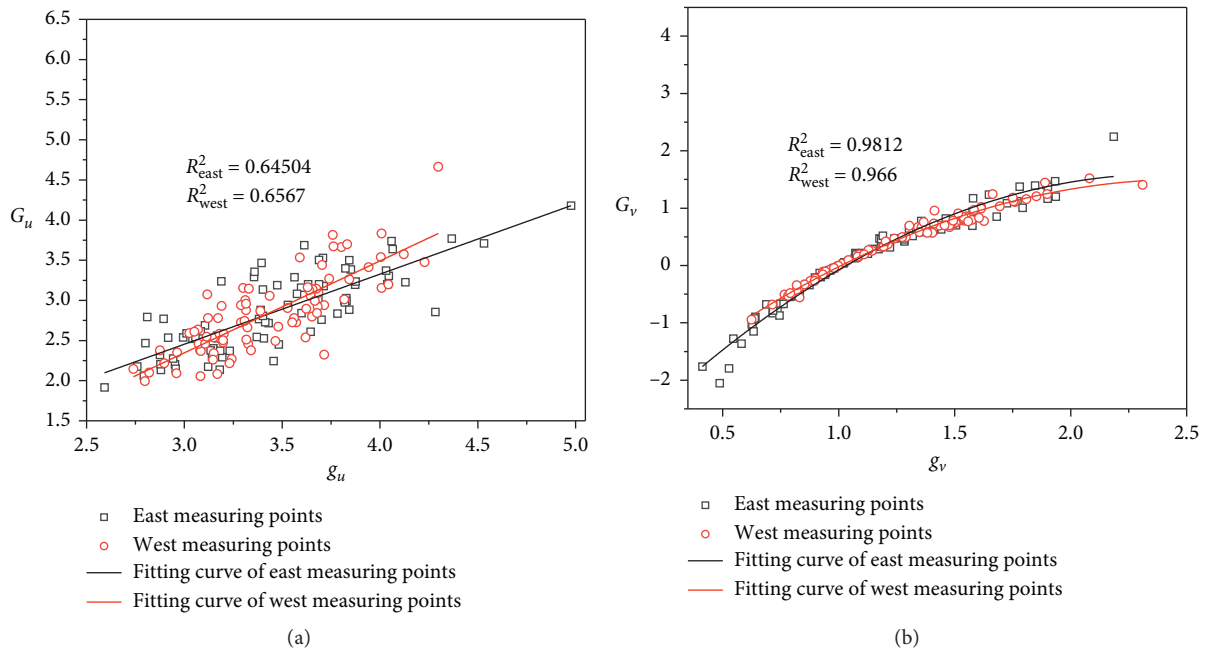

Figure 11: Variation of the gust factor with the peak factor. (a) Longitudinal. (b) Lateral.

Figure 12 shows the variation in the longitudinal and lateral attenuation coefficients with the mean wind speed. It is observed that the longitudinal and lateral attenuation coefficients exhibit discreteness with the mean wind speed, and a change law cannot be observed, which is consistent with data from Typhoon "Muifa" [43]. The average longitudinal and lateral attenuation coefficients are 10.71 and 7.43, respectively. The longitudinal attenuation coefficient is larger and the lateral attenuation coefficient is smaller than the corresponding results for Typhoon "Mei Hua."

Figure 13 shows the fitting of the measured longitudinal and lateral fluctuating wind coherence coefficients and empirical curves at the two sides. It is observed that the measured coherence coefficient of the fluctuating wind fits well with the empirical curve in both the longitudinal and lateral directions, indicating that Davenport's empirical

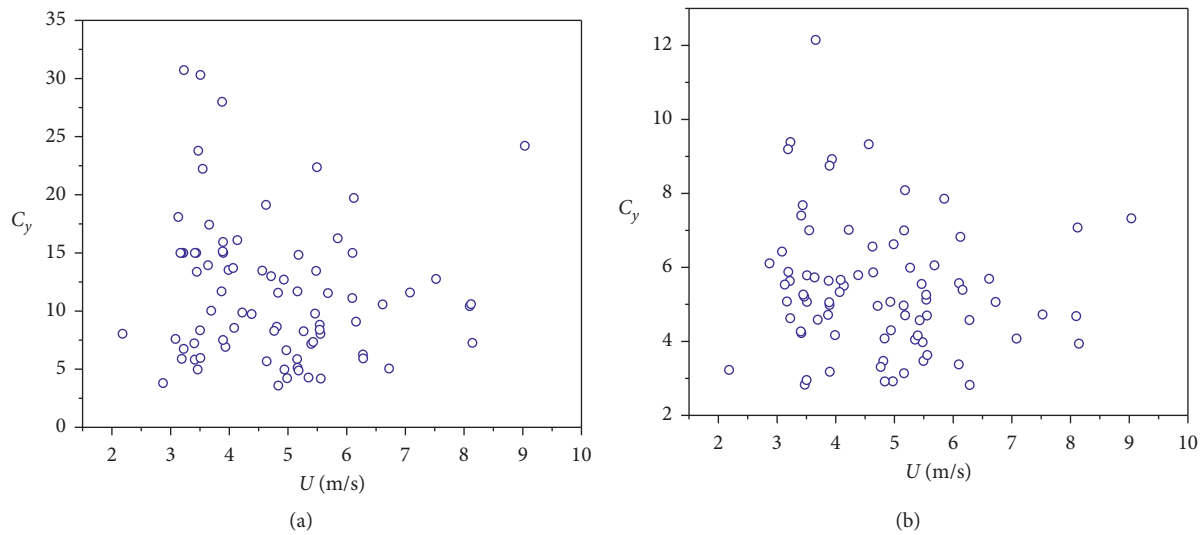

Figure 12: Variation of attenuation index with mean wind speed. (a) Longitudinal. (b) Lateral.

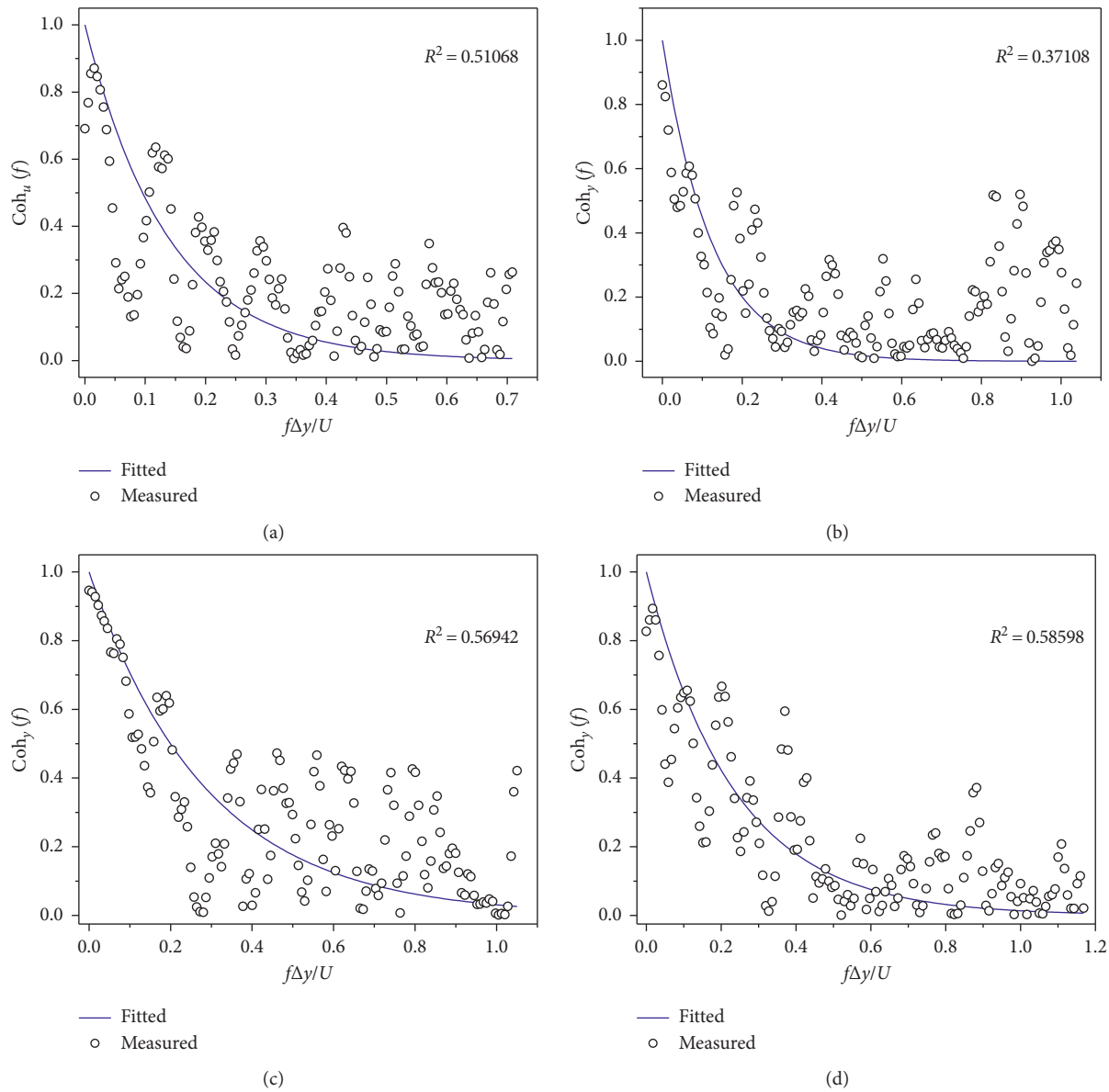

Figure 13: Continued.

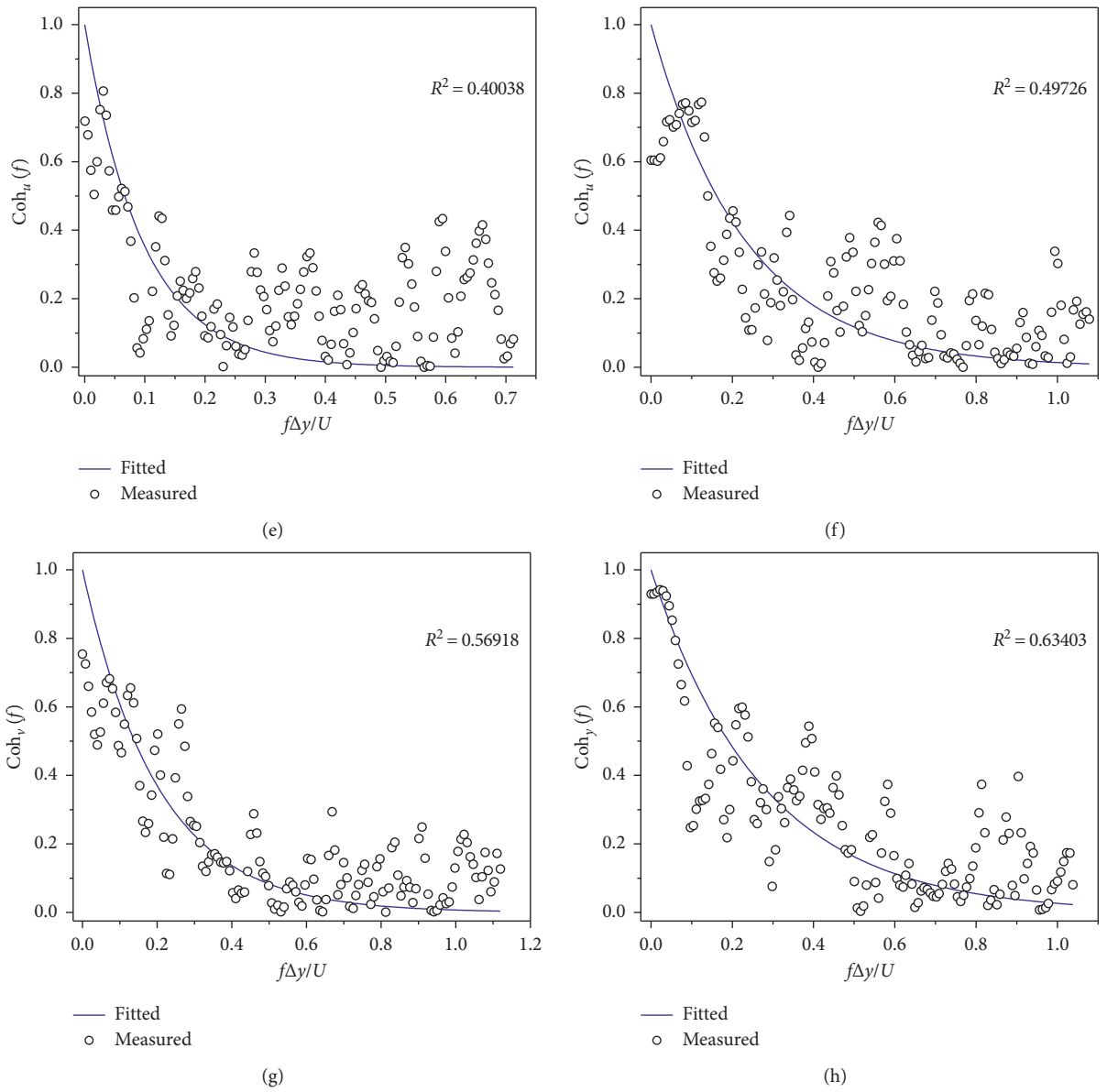

Figure 13: Coherence coefficient curves of lateral fluctuating wind speed component with different wind speeds. (a) Longitudinal measuring point 1. (b) Longitudinal measuring point 2. (c) Longitudinal measuring point 3. (d) Longitudinal measuring point 4. (e) Lateral measuring point 1. (f) Lateral measuring point 2. (g) Lateral measuring point 3. (h) Lateral measuring point 4.

formula (1961) can express the correlation characteristics of the fluctuating wind speed components of Typhoon Fung-Wong at the east and west measuring points.

3.6. Autocorrelation. Autocorrelation analysis determines the dependence of the instantaneous value at one time on the instantaneous value at another time in the same signal sequence. For a stationary signal process, the autocorrelation function and the time difference can be expressed as shown in the following equation:

$$R_{xx}(\tau) = E[X(t)X(t+\tau)], \tag{11}$$

where R_{xx}, τ, and $X(t)$ are the autocorrelation function, time difference, and time series, respectively.

Figure 14 shows the variation curves for the autocorrelation coefficients of the longitudinal and lateral fluctuating wind speed components at the east and west measuring points. The autocorrelation coefficient decreases with an increase in the time difference at the two measuring points, regardless of the longitudinal or lateral direction, indicating that the dependence of the instantaneous values at the two time points gradually decreases with an increase in the time difference. The decay rate of the longitudinal autocorrelation coefficient with a time difference is less than the decay rate of the lateral autocorrelation coefficient. The results show that the dependence of the longitudinal direction fluctuation

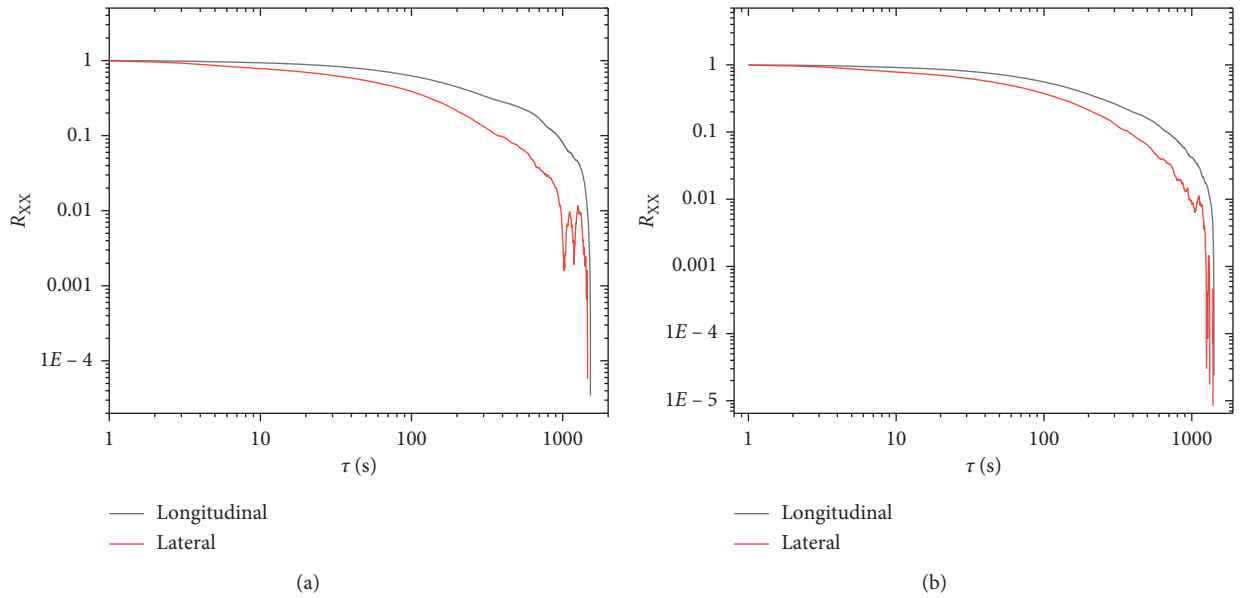

Figure 14: Fluctuating autocorrelation coefficient. (a) Longitudinal. (b) Lateral.

component at different times is stronger than that of the lateral direction fluctuation component.

4. Conclusion

Based on the analysis of Typhoon Fung-Wong in Wenzhou, the main findings of this study are summarized as follows:

(1) The results show that the longitudinal and lateral turbulence intensities decrease with an increase in the mean wind speed, and the discreteness of the west measuring points is greater than that of the east measuring points. The lateral turbulence intensity increases with an increase in the longitudinal turbulence intensity; there is an obvious positive correlation. With different wind speeds, the turbulence intensity decreases with an increase in wind distance, and the attenuation coefficient increases with a decrease in turbulence intensity.

(2) The longitudinal and lateral gust factors gradually decrease with an increase in the mean wind speed, and the decreasing trend is more obvious in the cross-wind direction. The longitudinal gust factor is significantly larger than the lateral gust factor. The longitudinal and lateral gust factors decrease with time, and the attenuation speed decreases with a decrease in the gust factor.

(3) The peak factors of the longitudinal and lateral arrays decrease with an increase in the mean wind speed, and the decreasing trend is more obvious in the cross-wind direction. There is a significant correlation between the gust factor and the peak factor. The vertical and horizontal fitting results for the two parameters are $G_u = 1.01g_u - 0.63$ and $G_v = -0.76g_v^2 + 3.72g_v - 3.01$, respectively.

(4) The average longitudinal and lateral attenuation coefficients of the east and west measuring points are 11.54 and 5.42, respectively. The measured coherence coefficients of fluctuating wind fit well with Davenport's empirical curve (1961) in both the longitudinal and lateral directions, indicating that Davenport's empirical curve can show the correlation characteristics of the fluctuating wind speed components of Typhoon Fung-Wong at the east and west measuring points.

(5) The dependence of the fluctuation component in the longitudinal direction is stronger than that in the lateral direction.

(6) Although the wind characteristics at the bridge site can be obtained from the field measured data, the value of one-time results is limited due to the strong randomness and fluctuation of wind. Therefore, it is of great significance to obtain wind characteristic database by long-term monitoring and research by wind tunnel test.

Data Availability

The data used to support the findings of this study are included within the article.

Conflicts of Interest

The authors declare that they have no conflicts of interest.

Acknowledgments

The work was supported by the State Key Laboratory of Mountain Bridge and Tunnel Engineering (SKLBT-19-001), Chongqing Engineering and Technology Research Center for Big Data of Public Transportation Operation

(no. 2019JTDSJ-ZD01), the Science and Technology Project Affiliated to the Education Department of Chongqing (KJQN201900103), the https://doi.org/10.13039/501100005230Natural Science Foundation of Chongqing, China (Grant nos. cstc2019jcyj-msxm0639 and cstc2020jcyj-msxmX0921), and the Key project of Technological Innovation and Application Development in Chongqing (Grant no. cstc2019jscx-gksb0188).

References

[1] B. Wang, F. Hu, and X. Cheng, "Wind gust and turbulence statistics of typhoons in South China," *Acta Meteorologica Sinica*, vol. 25, no. 1, pp. 113–127, 2011.

[2] W. H. Shi, Z. N. Li, and C. X. Zhang, "Field measurements of strong wind characteristics near ground in Wenzhou district," *Journal of Building Structures*, vol. 31, no. 10, pp. 34–40, 2010.

[3] H. Wang, A. Li, T. Guo, and J. Xie, "Field measurement on wind characteristic and buffeting response of the Runyang suspension bridge during typhoon matsa," *Science in China-Series E: Technological Sciences*, vol. 52, no. 5, pp. 1354–1362, 2009.

[4] H. Wang, Z. H. Zong, A. Q. Li, T. Tong, J. Niu, and W. P. Deng, "Digital simulation of 3D turbulence wind field of Sutong Bridge based on measured wind spectra," *Journal of Zhejiang University-Science*, vol. 13, no. 2, pp. 91–104, 2012.

[5] L. Song, J. Pang, C. Jiang, H. Huang, and P. Qin, "Field measurement and analysis of turbulence coherence for typhoon nuri at macao friendship bridge," *Science China Technological Sciences*, vol. 53, no. 10, pp. 2647–2657, 2010.

[6] J. Y. Fu, J. R. Wu, A. Xu, Q. S. Li, and Y. Q. Xiao, "Full-scale measurements of wind effects on guangzhou west tower," *Engineering Structures*, vol. 35, pp. 120–139, 2012.

[7] T. Tao, P. Shi, and H. Wang, "Spectral modelling of typhoon winds considering nexus between longitudinal and lateral components," *Renewable Energy*, vol. 162, pp. 2019–2030, 2020.

[8] T. Y. Tao, H. Wang, and K. Y. Zhao, "Efficient simulation of fully non-stationary random wind field based on reduced 2D hermite interpolation," *Mechanical Systems and Signal Processing*, vol. 150, Article ID 107265, 2021.

[9] T. Tao, H. Wang, L. Hu, and A. Kareem, "Error analysis of multivariate wind field simulated by interpolation-enhanced spectral representation method," *Journal of Engineering Mechanics*, vol. 146, no. 6, Article ID 04020049, 2020.

[10] H. A. Panovsky and A. D. Jhon, *Atmospheric Turbulence: Models and Methods for Engineering applications*, Wiley, Hoboken, NJ, USA, 1984.

[11] H. Liu, *Wind Engineering: A Handbook for Structural engineers*, Prentice-Hall, Englewood Cliffs, NJ, USA, 1991.

[12] S. Cao, T. Wang, Y. Ge, and Y. Tamura, "Numerical study on turbulent boundary layers over two-dimensional hills-effects of surface roughness and slope," *Journal of Wind Engineering and Industrial Aerodynamics*, vol. 104–106, pp. 342–349, 2012.

[13] T. Tamura, A. Okuno, and Y. Sugio, "LES analysis of turbulent boundary layer over 3D steep hill covered with vegetation," *Journal of Wind Engineering and Industrial Aerodynamics*, vol. 95, no. 9–11, pp. 1463–1475, 2007.

[14] L. Cochran and R. Derickson, "A physical modeler's view of Computational Wind Engineering," *Journal of Wind Engineering and Industrial Aerodynamics*, vol. 99, no. 4, pp. 139–153, 2011.

[15] P. Hu, Y. Li, Y. Han, S. C. S. Cai, and X. Xu, "Numerical simulations of the mean wind speeds and turbulence intensities over simplified gorges using the SST k-ω turbulence model," *Engineering Applications of Computational Fluid Mechanics*, vol. 10, no. 1, pp. 359–372, 2016.

[16] S. Iizuka and H. Kondo, "Performance of various sub-grid scale models in large-eddy simulations of turbulent flow over complex terrain," *Atmospheric Environment*, vol. 38, no. 40, pp. 7083–7091, 2004.

[17] S. Iizuka and H. Kondo, "Large-eddy simulations of turbulent flow over complex terrain using modified static eddy viscosity models," *Atmospheric Environment*, vol. 40, no. 5, pp. 925–935, 2006.

[18] J. E. Bullard, G. F. S. Wiggs, and D. J. Nash, "Experimental study of wind directional variability in the vicinity of a model valley," *Geomorphology*, vol. 35, no. 1-2, pp. 127–143, 2000.

[19] C. G. Li, Z. Q. Chen, Z. T. Zhang, and J. C. K. Cheung, "Wind tunnel modeling of flow over mountainous valley terrain," *Wind and Structures An International Journal*, vol. 13, no. 3, pp. 275–292, 2010.

[20] P. Hu, Y. Li, C. S. Cai, H. Liao, and G. J. Xu, "Numerical simulation of the neutral equilibrium atmospheric boundary layer using the SST k-ω turbulence model," *Wind and Structures*, vol. 17, no. 1, pp. 87–105, 2013.

[21] K. J. Eaton and J. R. Mayne, "The measurement of wind pressures on two-storey houses at Aylesbury," *Journal of Wind Engineering and Industrial Aerodynamics*, vol. 1, pp. 67–109, 1975.

[22] P. R. Sparks, G. T. Reid, W. D. Reid, S. Weish, and N. Weish, "Wind conditions in hurricane Hugo by measurement, inference, and experience," *Journal of Wind Engineering and Industrial Aerodynamics*, vol. 41, no. 1–3, pp. 55–66, 1992.

[23] N. Kato, T. Ohkuma, J. R. Kim, H. Marukava, and Y. Nilhori, "Full-scale measurements of wind velocity in two urban areas using an ultrasonic anemometer," *Journal of Wind Engineering and Industrial Aerodynamics*, vol. 41, no. 1–3, pp. 67–78, 1992.

[24] O. J. Andersen and J. Løvseth, "Gale force maritime wind. The Frøya data base. Part 1: sites and instrumentation. Review of the data base," *Journal of Wind Engineering and Industrial Aerodynamics*, vol. 57, no. 1, pp. 97–109, 1995.

[25] R. N. Sharma and P. J. Richards, "A re-examination of the characteristics of tropical cyclone winds," *Journal of Wind Engineering and Industrial Aerodynamics*, vol. 83, no. 1, pp. 21–33, 1999.

[26] M. C. H. Hui, A. Larsen, and H. F. Xiang, "Wind turbulence characteristics study at the stonecutters bridge site: Part I-Mean wind and turbulence intensities," *Journal of Wind Engineering and Industrial Aerodynamics*, vol. 97, no. 1, pp. 22–36, 2009.

[27] M. C. H. Hui, A. Larsen, and H. F. Xiang, "Wind turbulence characteristics study at the Stonecutters Bridge site: Part II: wind power spectra, integral length scales and coherences," *Journal of Wind Engineering and Industrial Aerodynamics*, vol. 97, no. 1, pp. 48–59, 2009.

[28] Q. S. Li, L. H. Zhi, J. Yi, A. To, and J. Xie, "Monitoring of typhoon effects on a super-tall building in Hong Kong," *Structural Control and Health Monitoring*, vol. 21, no. 6, pp. 926–949, 2014.

[29] H. Wang, T. Guo, T. Y. Tao, and A. Q. Li, "Study on wind characteristics of Runyang suspension bridge based on long-term monitored data," *International Journal of Structural Stability and Dynamics*, vol. 16, no. 4, Article ID 1640019, 2016.

[30] J. Zhang, M. Zhang, Y. Li, F. Jiang, L. Wu, and D. Guo, "Comparison of wind characteristics in different directions of deep-cut gorges based on field measurements," *Journal of Wind Engineering and Industrial Aerodynamics*, vol. 212, Article ID 104595, 2012.

[31] P. Liu, L. Zhao, G. Fang, and Y. Ge, "Explicit polynomial regression models of wind characteristics and structural effects on a long: pan bridge utilizing onsite monitoring data," *Structural Control and Health Monitoring*, vol. 28, no. 5, 2021.

[32] H. Li, S. Laima, J. Ou et al., "Investigation of vortex-induced vibration of a suspension bridge with two separated steel box girders based on field measurements," *Engineering Structures*, vol. 33, no. 6, pp. 1894–1907, 2011.

[33] Q. S. Li, J. R. Wu, S. G. Liang, Y. Q. Xiao, and C. K. Wong, "Full-scale measurements and numerical evaluation of wind-induced vibration of a 63-story reinforced concrete tall building," *Engineering Structures*, vol. 26, no. 12, pp. 1779–1794, 2004.

[34] Q. S. Li, Y. Q. Xiao, J. Y. Fu, and Z. N. Li, "Full-scale measurements of wind effects on the Jin Mao building," *Journal of Wind Engineering and Industrial Aerodynamics*, vol. 95, no. 6, pp. 445–466, 2007.

[35] Z. S. Chen, X. Fu, Y. Xu, C. Y. Li, B. Kim, and K. T. Tse, "A perspective on the aerodynamics and aeroelasticity of tapering: partial reattachment," *Journal of Wind Engineering and Industrial Aerodynamics*, vol. 212, Article ID 104590, 2021.

[36] Z. S. Chen, K. T. Tse, K. C. S. Kwok, A. Kareem, and B. Kim, "Measurement of unsteady aerodynamic force on a galloping prism in a turbulent flow: a hybrid aeroelastic-pressure balance," *Journal of Fluids and Structures*, vol. 102, Article ID 103232, 2021.

[37] M. Liu, H. L. Liao, M. S. Li, C. M. Ma, and M. Yu, "Long-term field measurement and analysis of the natural wind characteristics at the site of Xi-hou-men Bridge," *Journal of Zhejiang University-Science*, vol. 13, no. 3, pp. 197–207, 2012.

[38] Z. S. Chen, H. L. Huang, Y. M. Xu, K. T. Tse, and B. Kim, Y. T. Wang, "Unsteady aerodynamics on a tapered prism under forced excitation," *Engineering Structures*, vol. 240, Article ID 112387, 2021.

[39] F. Y. Xu, Z. Y. Ma, and H. Zeng, "A new method for studying wind engineering of bridges: large-scale aeroelastic model test in natural wind," *Journal of Wind Engineering and Industrial Aerodynamics*, vol. 202, Article ID 104234, 2020.

[40] F. Xu, C. Cai, and Z. Zhang, "Investigations on coefficient of variation of extreme wind speed," *Wind and Structures*, vol. 18, no. 6, pp. 633–650, 2014.

[41] H. Wang, Z. Zou, T. Tao, J. Mao, and X. Zd, "Comparative analysis on measured wind characteristics of typical typhoons at Sutong bridge," *Journal of Southeast University (Natural Science Edition)*, vol. 48, no. 2, pp. 342–349, 2018.

[42] A. G. Davenport, "Buffeting of a suspension bridge by storm winds," *Journal of the Structural Division*, vol. 88, no. 3, 1962.

[43] X. Wang, C. Huang, P. Huang, and X. Yu, "Study on wind characteristics of a strong typhoon in near-ground boundary layer," *The Structural Design of Tall and Special Buildings*, vol. 26, no. 5, pp. 1–13, 2017.